Coherent Photoproduction of Pions on Spin-Zero Nuclei in a relativistic, non-local Model * †

W. Peters‡, H. Lenske and U. Mosel

Institut für Theoretische Physik, Universität Giessen
D-35392 Giessen, Germany

Abstract

A relativistic and non-local model for the coherent photoproduction of pions on spin-zero nuclei is presented. The production operator is derived from an effective Lagrangian model that contains all the degrees of freedom known to contribute to the elementary process. Using the framework of DWIA, the matrix elements of this operator are evaluated using relativistic bound state wave functions. Final state interactions are accounted for via a pion-nucleus optical potential. The effects of in-medium modifications of the production operator are discussed. We give results for ^{12}C and ^{40}Ca, and compare our calculations to the data of the A2 collaboration at MAMI.

I. INTRODUCTION

Photonuclear reactions offer a unique possibility to test our understanding of hadrons in vacuum as well as within a nuclear environment. For elementary reactions like the photoproduction of pions on nucleons, relativistic models based on an effective Lagrangian approach are well established by now (see for example [1] and references therein). Starting from the elementary process, numerous studies treat the photoproduction of pions on nuclei. Among the large number of possible reactions, the coherent photoproduction plays a special role. Since in this case the nucleus remains in the ground state after the reaction process, the amount of further theoretical assumptions is smaller than e.g. in the case of reactions like $(\gamma, \pi N)$ or completely inclusive processes like photoabsorption on nuclei. In this sense the coherent photoproduction of pions is the cleanest test for any model that treats photoproduction of pions on nuclei.

---

*Work supported by BMBF and GSI Darmstadt.

†This work forms part of the dissertation of W. Peters.

‡Wolfram.Peters@theo.physik.uni-giessen.de

Data on the coherent photoproduction of pions on nuclei were published in [2]. The extraction of the coherent events in most of these experiments, however, was uncertain, so that comparison to these data is not very conclusive. More recently, the differential cross section was given for a photon energy of $E_\gamma \approx 175$ MeV in [3]. It is, however, a special feature of the coherent process, that the differential cross section is mainly sensitive to the nuclear form factor (see Sec. II C). Since the nuclear wave functions, and therefore the bound state properties of the nucleus, are taken as an input, all models yield more or less the correct shape of the differential cross section as can be seen in [3]. For a given energy they differ mainly with respect to the absolute value of the cross section. To further distinguish between different models, energy dependent data are needed. Thus the new data of the A2-collaboration at MAMI [4], which give the differential cross section at a fixed angle for a large energy range between 140 MeV and 430 MeV, are highly welcome. They enable us to test our calculations not only close to threshold, but over the entire Δ region.

Part of the existing calculations for the coherent photoproduction of pions work in the delta-hole model [5–13]. These calculations treat the Δ and pion dynamics in a very sophisticated manner, however, non-resonant contributions are normally neglected (See, however, [8,11,12]). While many other works use a local approximation, in [12] the non-locality of the process is treated explicitly. Another group of models is mainly used for the threshold region and employs the distorted wave impulse approximation (DWIA) [14–18]. These studies take into account the non-resonant contributions, but resort for technical reasons to non-relativistic and local approximations.

In this paper we present a relativistic, non-local approach to the coherent photoproduction of neutral pions on spin-zero nuclei in the framework of DWIA. The production operator is taken from an effective field theory, which describes the cross section for the production of neutral pions on nucleons well. The wave function of the outgoing pion is calculated using an empirical π-nucleus optical potential including s- and p-wave contributions. The bound state wave functions are extracted from a relativistic equation of motion with empirically determined scalar and vector potentials. We thus include resonant and non-resonant contributions to the production operator in a consistently relativistic manner, without non-relativistic or local approximations. We also study the effect of medium modifications of the production operator, especially in the Δ contribution. This approach enables us to test our understanding of the relativistic structure of the nuclear ground state and the production operator, though we resort to empirical models for the nucleus and the pion-nucleus interaction.

In the following section we first describe the elementary production operator we use. After some general remarks on the coherent photoproduction of pions, we then give the details of our model. Results for PWIA, as well as DWIA calculations are shown in Sec. III. We finally discuss the effects of in-medium modifications of the production operator. In Sec. IV the results of our study are summarized.

II. THE MODEL

A. The elementary operator

The diagrams contributing to the elementary process of photoproduction of neutral pions on a single nucleon are shown in Fig. 1: There are the direct and crossed nucleon graph, the direct and crossed Δ-graph and the graph containing the omega meson in the t-channel. There could in principle also be an analogous graph containing the rho meson, but due the smallness of the corresponding couplings it contributes only negligibly to the production of neutral pions [1]. We use the following interaction terms:

$$\begin{aligned}
\mathcal{L}_{\pi NN} &= -\frac{g_{_{\pi NN}}}{m_\pi}\,\overline{\psi}\,\gamma_5(\not{\partial}\vec{\pi})\,\vec{\tau}\,\psi \\
\mathcal{L}_{\gamma NN} &= -e\,\overline{\psi}\,\tfrac{1}{2}(1+\tau_3)\gamma_\mu\;\psi\,A^\mu \\
&\quad -\tfrac{1}{2}\,\mathrm{e}\,\frac{\kappa_p}{2m_{_N}}\,\overline{\psi}\,\tfrac{1}{2}(1+\tau_3)\,\sigma_{\mu\nu}\,\psi\,F^{\mu\nu} \\
&\quad -\tfrac{1}{2}\,\mathrm{e}\,\frac{\kappa_n}{2m_{_N}}\,\overline{\psi}\,\tfrac{1}{2}(1-\tau_3)\,\sigma_{\mu\nu}\,\psi\,F^{\mu\nu} \\
\mathcal{L}_{\pi N\Delta} &= \frac{g_{_{\pi N\Delta}}}{m_\pi}\,\overline{\psi}^\mu_\Delta\,(\partial_\mu\vec{\pi})\,\vec{T}\,\psi + \text{h.c.} \\
\mathcal{L}_{\gamma N\Delta} &= \frac{ieg_{_{\gamma N\Delta}}}{m_\pi}\,\overline{\psi}^\mu_\Delta\,\gamma^\nu\,\gamma_5\,T_3\,\psi\,F_{\mu\nu} + \text{h.c.} \\
\mathcal{L}_{\omega\pi\gamma} &= \frac{eg_{_{\omega\pi\gamma}}}{4m_\pi}\,\varepsilon_{\mu\nu\rho\sigma}\,(V^{\mu\nu}\,F^{\rho\sigma})\pi \\
\mathcal{L}_{\omega NN} &= -g^v_{\omega NN}\,\overline{\psi}\,\gamma_\mu\;\psi\,\omega^\mu \\
&\quad -\tfrac{1}{2}\,\frac{g^t_{\omega NN}}{2m_{_N}}\,\overline{\psi}\,\sigma_{\mu\nu}\,\psi\,V^{\mu\nu} \quad ,
\end{aligned} \tag{1}$$

with $F_{\mu\nu}=\partial_\mu A_\nu-\partial_\nu A_\mu$ and $V_{\mu\nu}=\partial_\mu\omega_\nu-\partial_\nu\omega_\mu$, where $A_\mu(\omega_\mu)$ denotes the photon (omega) field.

For the Δ-propagator we take [19]:

$$G^{\mu\nu}_\Delta(p) = \mathrm{i}\,\frac{\not{p}+m_\Delta}{s-m^2_\Delta+\mathrm{i}\sqrt{s}\,\Gamma(s)}\,\Lambda^{\mu\nu} \tag{2}$$

with

$$\Lambda^{\mu\nu} \;=\; \left(g^{\mu\nu}-\frac{1}{3}\gamma^\mu\gamma^\nu-\frac{2}{3m^2_\Delta}p^\mu p^\nu-\frac{1}{3m_\Delta}(\gamma^\mu p^\nu-p^\mu\gamma^\nu)\right) \quad . \tag{3}$$

The width of the Δ is taken to depend on the energy:

$$\Gamma(s)=\Gamma_o\frac{m_\Delta}{\sqrt{s}}\left(\frac{q}{q_o}\right)^3\left(\frac{q_o^2+c^2}{q^2+c^2}\right)^2 \tag{4}$$

with $\Gamma_o = 120$ MeV and $c = 0.5$ GeV. q and q_o denote the momentum of the pion resulting from a decay of a Δ of a mass $\sqrt{s}$ and of 1.232 GeV, respectively, in the rest-frame of the Δ.

For the coupling constants we use the following values:

$$\begin{array}{llll} e & = 0.3028 \ , & g_{\pi NN} & = 0.97 \\ \kappa_p & = 1.79 \ , & \kappa_n & = -1.91 \\ g_{\pi N\Delta} & = 2.1 \ , & g_{\gamma N\Delta} & = 0.337 \\ g_{\omega\pi\gamma} & = 0.313 \ , & g^v_{\omega NN} & = 10 \\ g^t_{\omega NN} & = 1.4 \ . & & \end{array} \tag{5}$$

The coupling constants of the photon and the pion to the nucleon are well known. The value we use for $g_{\pi N\Delta}$ corresponds to an on-shell decay width of the Δ of 120 MeV, so that it is consistent with Γ_o in Eq. (4). $g_{\omega\pi\gamma}$ has been determined from the decay width of an omega meson into a pion and a photon [1]. For the couplings of the omega to the nucleon different values are used in the literature; the values given in (5) are taken from [20]. The contribution of the omega graph to the photoproduction of pions or eta mesons is small, so that the ωNN coupling constants cannot be determined by fitting the experimental data for these processes [21,22]. Instead, they are taken from NN scattering [23], or they are derived from the ρNN parameters via $SU(3)$ considerations [24]. The values for $g^v_{\omega NN}$ used in the literature for photoproduction processes range from 8 [24] to 17 [25]. In addition, a form factor is introduced at the ωNN-vertex:

$$F(t) = \frac{\Lambda^2 - m_\omega^2}{\Lambda^2 - t} \quad , \tag{6}$$

with $\Lambda^2 = 2$ GeV^2 [21]. The sensitivity of our results to the omega parameters will be discussed in Sec. III.

Finally, $g_{\gamma N\Delta}$ and c in Eq. (4) were determined by comparing the results of the present model to the data for the cross section of the photoproduction of neutral pions on protons [26]. As can be seen from Fig. 2, the differential cross section can be well reproduced with the parameters given above. We did not use multipoles for the determination of these parameters, since multipoles are especially sensitive to unitarization effects, which are not included in the present model.

B. Photoproduction on the nucleus

After having specified the elementary production operator we now turn to the photoproduction on the nucleus. The framework commonly used for exclusive processes like the coherent photoproduction is the DWIA. Here it is assumed that the production process involves only a single nucleon, while for the distortions of in- or outgoing particles interactions with the entire nucleus are taken into account. Thus many-body contributions to the production process are not taken into account. The single-particle production operator is taken from an elementary model and evaluated using relativistic bound state and scattering wave functions instead of plane waves. Since the nucleon participating in this reaction is bound

in a potential, it is off-shell, and the production operator must be evaluated for kinematical situations different from the one in the free case.

For technical reasons a relativistic production operator is often simplified using on-shell relations [27] or a non-relativistic reduction [25], in order to make its evaluation easier. The resulting production operators are more or less equivalent on-shell, but the off-shell behavior is not the same as for the original operator. To avoid this problem, we take the production operator in its original form from the model described in the previous section, without rewriting it. Thus we use the natural off-shell dependence resulting from an effective field theory.

A numerical complication arises from the fact that the production operator depends on the momentum of the struck nucleon, i.e. it is non-local. To circumvent complicated integrations, most DWIA calculations evaluate the production operator in a local approximation at some fixed effective nucleon momentum. For knock-out processes like $(\gamma, \pi N)$ the asymptotic momenta of the outgoing particles can be used to estimate the momentum arguments of the production operator. In the case of coherent production, however, both the incoming and the outgoing nucleon are in a bound state, so that they do not have a well defined asymptotic momentum. The validity of the local approximation for the photoproduction of charged pions is is discussed in [28,29]. To avoid the uncertainties related to the local approximation, we evaluate the matrix elements of the production operator non-locally. We will discuss the local and the non-relativistic approximation further in Sec. III.

C. The coherent process

In the nuclear coherent photoproduction of pions, the nucleus remains in the ground state after the reaction. Since the pion in the final state has the quantum numbers 0^-, the Lorentz invariant amplitude for the entire process must have the form [27]:

$$T^{(\lambda)} = \varepsilon_\mu^{(\lambda)} \, T^\mu \tag{7}$$

with

$$T^\mu = \varepsilon^{\mu\nu\rho\sigma} \, k_\nu \, p_\rho \, q_\sigma \;\; A(s,t) \quad . \tag{8}$$

k, p and q are the momenta of the incoming photon, the incoming nucleus and the outgoing pion, respectively. $\varepsilon_\nu^{(\lambda)}$ is the polarization vector of the photon and $A(s,t)$ is a scalar function that contains the entire dynamics of the process and depends on the Mandelstam variables s and t. This can be shown to yield:

$$\sum_\lambda \mid T^{(\lambda)} \mid^2 = \; W^2 \, k_{cm}^2 \, q_{cm}^2 \sin^2\theta_{cm} \mid A(s,t) \mid^2 \quad . \tag{9}$$

k_{cm}^2 and q_{cm}^2 are the three momenta of the photon and the pion, θ_{cm} is the scattering angle and W is the total energy of the photon-nucleus system; all these quantities are taken in the cm-frame. Thus the well known $\sin^2\theta$-dependence of the coherent photoproduction of pions results directly from the quantum numbers involved. The differential cross section in the cm-frame is then given by:

$$\frac{d\sigma}{d\Omega} \;=\; \left(\frac{M_A}{4\pi W}\right)^2 \frac{q_{cm}}{k_{cm}} \frac{1}{2} \sum_{\lambda} \mid T^{(\lambda)} \mid^2 \quad , \tag{10}$$

where M_A is the mass of the nucleus.

Another important consequence of Eq. (7) is, that if one replaces the photon polarization ε_μ by the photon momentum k_μ, $T^{(\lambda)}$ vanishes. Thus the amplitude $T^{(\lambda)}$ is gauge invariant from the very beginning, independent of the model used for the nuclear ground state or the production process. This is a special feature of the coherent photoproduction on spin-zero nuclei, which makes this reaction even more attractive from a theoretical point of view: In other reactions than the coherent one, like $(\gamma, \pi N)$ or $(e, e'N)$, the usual DWIA approach leads to a gauge-dependent amplitude [30–32]. Methods to restore gauge invariance lead to theoretical uncertainties [31], which do not occur in the case of coherent photoproduction.

We work in position space, since the bound state and scattering state wave functions can easily be obtained in a position space representation. In the approach described above the first diagram in Fig. 1 corresponds to the following non-local expression:

$$T^{(\lambda)}_{Ndir} = \sum_{\alpha \; occ.} \int d^3x \, d^3y \, \overline{\psi}_\alpha(\vec{x}) \, \phi_\pi^{(-)^*}(\vec{x}) \, \Gamma_{\pi NN} \, G^o_N(E; \vec{x}, \vec{y}) \, \Gamma^\mu_{\gamma NN} \, \phi^{(\lambda)}_\mu(\vec{y}) \, \psi_\alpha(\vec{y}) \quad . \tag{11}$$

Here ψ_α is the wave function of the bound nucleon, $\phi^{(\lambda)}_\mu$ is the wave function of the photon, which can be assumed to be a plane wave and $\phi^{(-)}_\pi$ is the distorted wave function of the pion satisfying incoming boundary conditions [33]. $\Gamma_{\pi NN}$ and $\Gamma^\mu_{\gamma NN}$ are the vertices resulting from the coupling terms in Eq. (1) and G^o_N is the free nucleon propagator:

$$G^o_N(E; \vec{x}, \vec{y}) = \int \frac{d^3p}{(2\pi)^3} \, \frac{\mathrm{i} e^{\mathrm{i}\vec{p}(\vec{x}-\vec{y})}}{\not{p} - m} \quad . \tag{12}$$

The effect of including a dressed instead of a free nucleon propagator will be discussed in Sec. III C. E is naturally determined by energy conservation:

$$E = E_\gamma + E_\alpha \quad , \tag{13}$$

where E_α is the total, relativistic energy of the bound nucleon.

To evaluate (11), we use partial-wave expansions for the wave functions as well as for the propagator [33]. Whenever derivatives appear in the vertices, we actually insert the derivatives of wave functions, so that we take into account the non-locality of the production operator. After inserting the partial-wave expansions into Eq. (11) we can perform the angular integrations analytically, since they only involve spherical harmonics. The two radial integrations are evaluated numerically.

The remaining graphs in Fig. 1 are treated analogously. For the Δ-propagator we treat the contraction of $\Lambda_{\mu\nu}$ from Eq. (3) with the $\Delta N\gamma$-vertex as one term and use the partial-wave expansion only for the remaining spin-$\frac{1}{2}$ part of the propagator:

$$\frac{\not{p} + m_\Delta}{s - m^2_\Delta + \mathrm{i}\sqrt{s}\,\Gamma(s)} \quad , \tag{14}$$

by taking its Fourier transform analogously to Eq. (12). However, a closed expression of this Fourier transform, which is needed in order to use the formula for a partial wave expansion,

can only be obtained if the imaginary part of the denominator does not depend on the three-momentum $\vec{p}$. Since $s\,\Gamma(s)$ depends on $\vec{p}$ via $s = p_o^2 - \vec{p}^{\,2}$, we evaluate this term at a value $s_o(E_\gamma, E_\alpha)$, which is taken to be the invariant mass of a system of the photon and the struck nucleon, averaged over the Fermi-sphere. Consequently, the Δ-width is a function of the energy of the incoming photon (E_γ) and the struck nucleon (E_α) .

A further technical problem arises from the $p_\mu\, p_\nu$ term in Eq. (3), since its spatial components $p_i\, p_j$ contain second derivatives, an exact treatment of which would greatly complicate the calculations. We therefore approximate this term by replacing

$$p_i\, p_j \;\rightarrow\; k_i\, k_j \quad , \tag{15}$$

where k is the three-momentum of the photon. Since in momentum space the three-momentum of the Δ-propagator is the sum of photon and nucleon momentum, this amounts to putting for this special term the three-momentum of the incoming nucleon to zero. Using this approximation, this term contributes only on the percent level, thus affecting our results insignificantly.

The ωNN form factor in Eq. (6) is approximated by using the asymptotic momentum of the pion in $t = (p_\gamma - p_\pi)^2$. In the relevant kinematic region, t is small anyway as compared to the cutoff Λ^2. Consequently the dependence of $F(t)$ on the pion distortions is weak and its main effect is a renormalization of the ωNN coupling.

The angular integrations in Eq. (11) lead to rather complicated expressions for the vertices depending on the incoming and outgoing angular momenta. The $\sin\theta$ dependence of the differential cross section is one test for their correct numerical implementation. As a further test we have checked that for T^μ from Eq. (8) our calculation yields:

$$T_o = 0;\; T_i\, k_i = 0 \quad , \tag{16}$$

which has to be fulfilled for each graph separately, as can be seen from the definition of this quantity.

Even though we evaluate the amplitude in position space it is instructive to consider Eq. (11) in momentum space:

$$\begin{aligned} T_{Ndir} &= \sum_{\alpha\; occ.} \int \frac{d^3p}{(2\pi)^3}\, \overline{\psi}_\alpha(\vec{p}+\vec{k}-\vec{q})\, \Gamma_{\pi NN}\, G_N(E;\vec{p}+\vec{k})\, \Gamma_{\gamma NN}\, \psi_\alpha(\vec{p}) \\ &= \sum_{\alpha\; occ.} \int \frac{d^3p}{(2\pi)^3}\, \overline{\psi}_\alpha(\vec{p}+\vec{k}-\vec{q})\, \hat{T}_{Ndir}(E;\vec{p},\vec{k},\vec{q})\, \psi_\alpha(\vec{p}) \quad , \end{aligned} \tag{17}$$

where for the moment we assume the pion wave function to be a plane wave. If we now make the local approximation as described at the end of Sec. II B by putting the momentum of the incoming nucleon in the argument of $\hat{T}_{Ndir}$ equal to a constant $\vec{p}_o$, we can rewrite Eq. (17):

$$T_{Ndir} \approx Tr\left(\hat{T}_{Ndir}(E;\vec{p}_o,\vec{k},\vec{q})\;\; \hat{\rho}_A(\vec{k}-\vec{q})\right) \quad , \tag{18}$$

with the density matrix:

$$\hat{\rho}_A(\vec{p}) = \int \frac{d^3p'}{(2\pi)^3} \sum_{\alpha\ occ.} \psi_\alpha(\vec{p'}) \otimes \overline{\psi}_\alpha(\vec{p'} + \vec{p})$$
$$= \int d^3x\ \mathrm{e}^{\mathrm{i}\vec{p}\vec{x}} \sum_{\alpha\ occ.} \psi_\alpha(\vec{x}) \otimes \overline{\psi}_\alpha(\vec{x}) = \int d^3x\ \mathrm{e}^{\mathrm{i}\vec{p}\vec{x}}\ \hat{\rho}_A(\vec{x}) \quad . \tag{19}$$

The density matrix $\hat{\rho}_A(\vec{x})$ contains the complete information about the nuclear ground state. The scalar, vector and tensor densities are obtained by taking $Tr(\Gamma\hat{\rho}_A)$ with $\Gamma = 1, \gamma_o, \sigma^{0i}$, respectively. This is in contrast to the approach used in [27] for the coherent photoproduction of η-mesons. There the production operator is rewritten using the free Dirac equation for in- and outgoing nucleons. As a consequence, the coherent photoproduction of η-mesons depends in [27] only on the tensor density of the nuclear ground state.

One sees from Eqs. (18) and (19), that in the local approximation the differential cross section for coherent photoproduction at a fixed energy involves the Fourier transformation of a nuclear ground state density, i.e. a nuclear form factor. Although effects due to the non-locality of the production operator and the distortions of the pion wave function by the nucleus are superimposed, the differential cross section is dominated by the nuclear form factor. Hence the properties of the production operator itself can only be studied when the energy dependence of the cross section is considered.

D. The nuclear wave function

It is clear from these considerations, that it is crucial to describe the ground state properties of the nucleus realistically. The wave functions in Eq. (11) are taken from a relativistic mean-field calculation using scalar and time-like vector potentials V_s and V_v, respectively:

$$(\not{p}\ -\ m\ -\ V_v\gamma_o\ -\ V_s)\psi_\alpha\ =\ 0 \quad . \tag{20}$$

For the potentials V^v and V^s we assume a Woods-Saxon shape:

$$V(r)\ =\ V_i^o\ \left(1\ +\ \mathrm{e}^{\frac{(r-r_i A^{1/3})}{a_i}}\right)^{-1} \quad ; i = v, s \quad . \tag{21}$$

The parameters we use for these potentials are given in Table I. They were determined such that the separation energies [34], the root mean square radius of the charge density and the charge form factors of ^{12}C and ^{40}Ca [35] are well reproduced. The resulting charge form factors are shown in Figs. 3 and 4, together with the values extracted from experiment [35].

By using these wave functions, we neglect higher order correlations beyond mean field dynamics. The question arises, to what extent the momentum structure of the nuclear ground state wave functions is adequately described by mean- field dynamics [36,37]. The coherent production process leaves the nucleus in the ground state and probes, in the energy range considered here, primarily momenta inside the Fermi-sphere. Thus, a reliable description of nuclear form factors in a momentum range up to about twice the Fermi-momentum is most important. As seen in Figs. 3 and 4, the measured charge form factors are indeed well reproduced up to a momentum transfer of about 3 fm^{-1}, so that the relevant momentum range is obviously well described. Extended approaches (e.g. [38,39]) are in fact showing

that for spherical nuclei deviations from mean-field dynamics will become detectable only at rather high momenta corresponding to short-range processes which are not considered here. A mean field version of the Walecka model has recently been used to treat the coherent photoproduction of η-mesons on nuclei [27].

E. The pion-nucleus interaction

It is well known, that the coherent cross section depends strongly on the interaction of the produced pion with the nucleus. This is taken into account by using a distorted pion wave function in Eq. (11), which is calculated from a position space optical potential. An optical potential as given in [40,41] is used:

$$\begin{aligned} 2E_\pi U_{opt}(r) = & -4\pi[b(r)+B(r)] \\ & +4\pi\vec{\nabla}\{L(r)[c(r)+C(r)]\}\vec{\nabla} \\ & -4\pi\left[\frac{p_1-1}{2}\nabla^2 c(r)+\frac{p_2-1}{2}\nabla^2 C(r)\right] \quad , \end{aligned} \tag{22}$$

where

$$\begin{aligned} b(r) &= p_1 b_o \rho(r) \\ c(r) &= p_1^{-1} c_o \rho(r) \\ B(r) &= p_2 B_o \rho^2(r) \\ C(r) &= p_2^{-1} C_o \rho^2(r) \\ L(r) &= \left\{1+\frac{4\pi}{3}\lambda[c(r)+C(r)]\right\}^{-1} \quad , \end{aligned}$$

with

$$p_1 = 1+\frac{E_\pi}{m_N}; \quad p_2 = 1+\frac{E_\pi}{2m_N} \quad . \tag{23}$$

E_π is the total energy of the pion, m_N is the mass of the nucleon and ρ is the nuclear density normalized to A, obtained by summing the single particle densities in the potentials Eq. (21) over the occupied states. This optical potential contains s- and p-wave interactions of the pion via $b(r)$ and $c(r)$ and the so called true absorption via $B(r)$ and $C(r)$. The quantity $L(r)$ comes in because of the Lorentz-Lorenz-Ericson-Ericson effect [19]. The last term in Eq. (22) results from the so called angle transformation [19], which is a kinematical effect. The parameter λ is a real constant, while the quantities b_o, c_o, C_o, and C_o are complex and energy dependent. In [40,41] these parameters are only given for pion kinetic energies up to 50 MeV. Since we want to compare our calculations to the A2 data, we need an optical potential for pion kinetic energies up to about 300 MeV. In order to have a consistent parameterization over this range of energies, we adopt the same form as in Eq. (22) also for higher energies. The parameters were determined by fitting the elastic scattering data of pions on ^{12}C [42], including the nuclear Coulomb potential as done in [40].

Doing so one is confronted with the fact that there is a large redundancy between some of the parameters, especially between b_o and B_o and between c_o and C_o [43]. Consequently,

a naive fit of all parameters leads to unphysical values. We therefore put $B_o = 0$ and $C_o = 0$ and determine b_o and c_o as complex, effective parameters. In Fig. 5 we show the cross sections for elastic pion scattering on ^{12}C in comparison to the experimental data. In order to have one more set of parameters at higher energies, we included elastic pion scattering on ^{16}O at $T_\pi = 330$ MeV into the fitting procedure. For $T_\pi = 100$ MeV and $T_\pi = 157$ MeV, we were not able to find a parameter set that led to agreement with the data beyond the second minimum of the differential cross section, without showing discrepancies at smaller angles. In these two cases we chose the optical potential parameters such that the data are reproduced well for angles up to the second minimum. In order to obtain the optical parameters as smooth functions of the pion energy, we have interpolated our fit results as shown in Fig. 6.

We expect that the empirical potential thus obtained describes the final state interactions of the pion in the case of ^{12}C sufficiently well in an energy range from threshold up to the Δ-resonance. The structure of this potential is different from potentials that were obtained from microscopic calculations [40,44], for which we also show results in Fig. 5. We will compare the effects of our potential in the coherent photoproduction to the effects of potentials that were extracted from microscopic models in Sec. III B.

III. RESULTS

A. PWIA

The model described in the previous section was used to calculate differential and total cross sections for the coherent photoproduction of pions on nuclei. In Fig. 7 and Fig. 8 we show our results for the plane wave impulse approximation (PWIA), i.e. with a free outgoing pion. As has been discussed at the end of Sec. II C, the total cross section shows the resonant character of the elementary production operator, while the shape of the differential cross section results from the nuclear form factor (multiplied with $\sin^2\theta$). In Fig. 7 we also show the contributions of the different diagrams. Clearly, the Δ-resonance dominates the process, but the other diagrams lead to sizable corrections that should not be neglected. Note the destructive interference between the Born terms and the other graphs. The omega contribution comes mainly from the vector coupling of the omega (Eq. (1)), the tensor coupling contributes only negligibly.

In order to compare to the non-relativistic, local approach used in the previous DWIA calculations, we performed a local calculation using the non-relativistic reduction of the direct Δ-graph as given in [25], which has also been used in [15,17]. The direct Δ-graph accounts for most of the total cross section (see Fig. 7). In order to compare this to our result for the direct Δ-graph, we have used our set of parameters (Eq. (5)) including the energy dependent Δ-width from Eq. (4). The struck nucleon was assigned an energy equal to the average energy of a bound nucleon in ^{12}C (cf. Eq. (13)). The three-momentum $\vec{p}_i$ of the struck nucleon in the photon-nucleus cm-system was assumed to be

$$\vec{p}_i = -\frac{\vec{k}}{A} - \frac{A-1}{2A}(\vec{k} - \vec{q}) \quad , \tag{24}$$

which is often used in local DWIA calculations (see e.g. [17]). The nuclear form factor was taken to be the vector form factor resulting from our ground state calculation, which corresponds to the charge form factor shown in Fig. 3, corrected for the electromagnetic form factor of proton and neutron.

The result of this calculation for the direct Δ-graph is shown as the dotted curve Fig. 9 for ^{12}C together with the result of 'exact' calculations (solid curve). In [5,16] it is found that in a non-relativistic approach there are additional corrections due to the transformation between the photon-nucleus and the photon-nucleon cm-frame. In [5] it is shown that the inclusion of this transformation corresponds to multiplying the amplitude with a factor $m[(m + E_\gamma)\sqrt{1 - v^2}]^{-1}$, where m is the mass of the nucleon and v is the boost velocity from the photon-nucleus to the photon-nucleon cm-system. Including this factor in our non-relativistic, local calculation leads to the dashed curve in Fig. 9. It is an advantage of the relativistic approach that these effects are correctly included when the Lorentz invariant amplitude (Eq. (11)) is calculated.

The difference between the the solid and the dashed curve in Fig. 9 cannot uniquely be separated into relativistic and non-local effects. In order to study the influence of the relativistic nuclear structure we performed calculations where we assumed the free relations between the upper and lower components of the nuclear wave functions, which led only to a slight decrease of the solid curve in Fig. 9. The difference between the solid and the dashed curves in Fig. 9 is therefore a result of the relativistic, non-local treatment of the production operator. In a non-relativistic framework non-local effects have been shown to be important in the photoproduction of charged pions in [28,29].

B. DWIA

We now take the final state interaction of the pion with the nucleus into account by means of the optical potential described in Sec. II E. The resulting total and differential cross sections for ^{12}C and ^{40}Ca are shown in Figs. 10, 11 and 12 in comparison to PWIA results. For the case of ^{40}Ca we took the same parameters for the pion optical potential as for ^{12}C. For $E_\gamma \lesssim 230$ MeV, i.e. for $T_\pi \lesssim 100$ MeV, where the absorption is relatively small (cf. Fig. 6), the distortion of the pion wave function leads to an increase of the total cross section, indicating the importance of off-shell effects in the pion distorted wave. For higher photon energies the cross section is strongly reduced because of the large imaginary part of the pion optical potential. This reduction is stronger in the case of ^{40}Ca, since the absorption of pions increases with the nuclear mass. Besides that, the curves for the two different nuclei are very similar in shape, and differ mainly by a global factor. Making an ansatz $\sigma \sim A^\alpha$ we find $\alpha \sim 0.7$-0.8 for the case of PWIA. This rather weak A-dependence results from the different momentum dependence of the nuclear form factor for ^{12}C and ^{40}Ca (cf. Figs. 3 and 4): For a given momentum transfer, the ^{40}Ca form factor is much smaller than the one for ^{12}C, which compensates for the fact that there are A amplitudes to be summed for a given nucleus (Eq. (11)). For the DWIA results we find $\alpha \sim 0.5$-0.7, depending on the photon energy, which reflects the pion absorption.

In Fig. 13 the result of a DWIA calculation for ^{12}C is compared to the A2 data. The position of the maximum in the data is well reproduced, but the height of this maximum is

underestimated by more than a factor of two. Before we turn to improvements of the DWIA calculation, we want to explore two possible sources of uncertainty.

First one has to be aware that two different but phase-equivalent optical potentials might yield the same elastic scattering cross section, but lead to a different behavior of the pion wave function in the nuclear interior [45]. Since in Eq. (11) the pion wave function within the nucleus, rather than its asymptotic behavior, is relevant, two phase equivalent optical potentials might in principle lead to different cross sections for the coherent photoproduction of pions.

In order to explore this ambiguity, we have also performed calculations using the optical potential of [44] and of [40,41]. As can be seen from Fig. 5, these potentials yield pion elastic scattering cross sections that are, in the respective energy ranges, comparable to the ones obtained with our optical potential. In [44] the results of a microscopic Δ-hole model calculation for the Δ-resonance in nuclear matter [46] have been used to construct a position-space optical potential for the pion. In Fig. 14 we show the result of a calculation employing this optical potential as well as our result in DWIA and PWIA. Both potentials lead to a rather similar behavior of the cross section, especially at higher photon energies. For the total cross sections, the agreement between calculations employing these two different optical potentials is qualitatively the same as for the differential cross section in Fig. 14. We have also performed calculations with the parameter sets given in [40] and [41] for $T_\pi =$ 50 MeV ($E_\gamma = 184$ MeV). Using these parameter sets, in which the parameters B_o and C_o are non-zero, we get a total cross section that differs from the one obtained with our pion optical potential by less than 10 % at this specific pion energy. We thus conclude, that our empirical parameterization for the pion optical potential accounts for the essential features of the pion nucleus interaction in the case of ^{12}C and ^{40}Ca.

As mentioned above, the ωNN vector coupling constant and the form factor (Eq. (6)), which lead to the ω contribution in Fig. 7, are not accurately known. In the elementary photoproduction of neutral pions the contribution of the omega graph to the differential cross section is about 10 %, depending on the angle. To show the dependence of our result for the coherent photoproduction on the omega parameters, we show in Fig. 15 calculations employing different values of $g^v_{\omega NN}$ and Λ. The values $g^v_{\omega NN} = 17$ and $g^v_{\omega NN} = 8$ represent the upper and lower bound of possible values for this coupling. The resulting uncertainty in our results is much smaller than the discrepancy between our DWIA results and the A2 data.

C. Medium effects

By using an optical potential to determine the distorted wave function of the pion, we already include the effect of the interaction of the produced pion with the nucleus. The intermediate particles contributing to the production operator, however, also interact with the nuclear medium.

For the nucleon propagator we include the resulting medium effects by replacing the free propagator with the one obtained from the mean-field in which the bound state wave functions were calculated. We thus employ a dressed nucleon propagator G_N that fulfills

$$(\not{p} \; - \; m \; - \; V_v\gamma_o \; - \; V_s)G_N(p_o;\vec{x},\vec{y}) \; = \; \mathrm{i}\delta^3(\vec{x}-\vec{y}) \quad . \tag{25}$$

Since G_N is calculated in the mean-field approximation, it contains the static properties of a struck nucleon interacting with the residual nucleus. Although it can certainly not account for the full dynamics of the struck nucleon interacting with the residual nucleus, it is the natural extension of the elementary model to reactions on the nucleus, in which the bound and the intermediate nucleon are treated consistently. In Fig. 16 we show results of calculations for ^{12}C using the free as well as the dressed nucleon propagator from Eq. (25). The increase of the cross section results from the fact, that the total contribution of the nucleon terms is the result of an approximate cancellation of direct and exchange graph. In the case of the dressed nucleon propagator, this cancellation is more complete, leading to a smaller net contribution. Because of the destructive interference of the Born terms with the other contributions, this leads to a larger cross section.

For the Δ-resonance we can use the Δ-hole model as a guideline. In [10,11] it is shown, that the medium modifications of the Δ, in addition to a distortion of the pion, have a clear effect on the coherent cross section. It is well known, that the Δ feels an attractive potential of about -30 MeV at normal nuclear density [19], which has an effect on any production process involving the Δ. Indeed, in (^{3}He$, t$) and (d,^{2}He) reactions a shift of the Δ-peak relative to the reaction on the proton has been observed [47,48]. A considerable part of this shift is, however, due to trivial effects e.g. the energy dependence of the nuclear form factor, so that it is only partially a consequence of in-medium modifications of the Δ [49,50]. In contrast to that, the Δ-peak remains essentially unshifted in the photoabsorption on nuclei [51].

Calculating the full, relativistic Δ-propagator in the presence of nuclear potentials is out of the scope of this work. We take the attractive self-energy of a Δ within a nucleus schematically into account by shifting its mass in the production operator. In Fig. 16 we also show the result of a calculation with the Δ-mass reduced by 30 MeV (full line). A mass shift of the Δ increases the cross section at lower energies and decreases it at higher energies. The value $\delta m_\Delta = -30$ MeV has been chosen such that the absolute height of the maximum of the A2 data is reproduced (Fig. 17). Since this number can only be interpreted as an average over the entire nucleus, it seems somewhat large in comparison to the depth of the Δ-potential of 30 MeV [19]. It must at this point also be kept in mind, that the actual value of δm_Δ needed to fit the data depends to some extent on the value used for of the ωNN coupling constant.

Besides the mass, the width of the Δ is also modified in the medium. A simple analysis taking into account Pauli blocking and collisional broadening leads to a width that is rather independent of the nuclear density [52], but delta-hole calculations yield a Δ self-energy, which corresponds to an increase of the width by as much as 60 MeV [46]. Including this effectively by adding a constant shift of 30 MeV to the energy dependent Δ-width in Eq. (4) changes the result depicted in Fig. 17 only at energies beyond the maximum, where the cross section is rather small. Thus for the A2 data we can clearly distinguish between the effect of a modified mass and a modified width of the Δ.

This procedure, to take into account the distortions of the produced pion via an optical potential and then include medium modifications of the intermediate Δ by changing its mass and its width independently, mimics the essentials of the Δ-hole model. The qualitative agreement with the Δ-hole model can also be seen in [10], where the amplitude for the coherent photoproduction of pions in the Δ-hole model is rewritten in such a way, that it

contains a distorted pion wave function and a modified Δ-propagator. In this study it is found, that the modifications of the Δ-propagator, in addition to the pion distortions, have considerable effects.

As can be seen in Fig. 17, the inclusion of a dressed nucleon propagator and a lowered Δ-mass leads to agreement of our calculation with the data around the maximum. At higher energies, the situation is not clear. The in-medium production operator seems to lead to an underestimation of the data for $E_\gamma > 350$ MeV. More experimental data, especially at smaller angles, are needed in this energy range before definite conclusions can be drawn.

Since there is no reliable information available on the properties of an ω-meson at space-like momenta in nuclear matter, we did not consider in-medium modifications of the ω-graph.

The special energy dependence of the differential cross section at a constant angle is the result of an interplay between the energy dependence of the production operator and the nuclear form factor. In order to circumvent the energy dependence of the form factor, and to eliminate the trivial $\sin^2\theta$ term (Eq. (9)), we show in Fig. 18 the differential cross section for a constant momentum transfer $|\vec{q}| = 0.1$ GeV, divided by $\sin^2\theta$ as a function of the photon energy for ^{12}C and ^{40}Ca. When plotting the cross section this way, the effects of in-medium modifications of the production operator are magnified and become visible over a large range of energies. Especially an increased Δ-width now leads to a pronounced effect. Thus the new TAPS data, that will cover a large range of angles for each energy [53], will provide an opportunity to test our method of treating medium effects further.

In order to also compare to calculations using the Δ-hole model, we show in Fig. 19 the total cross section for ^{12}C using a medium modified production operator taking all graphs into account, as well as that obtained by only including the direct Δ-term. The result for the direct Δ term agrees qualitatively with results of Δ-hole calculations. As compared to the most recent publications using the Δ-hole model [5,6], the height of the maximum in the cross section is in our model about the same as in [6], but somewhat above the result of [5]. The position of the maximum is, however, around E_γ=220 MeV in [5,6], compared to 260 MeV in our model. In [10,12] the Δ-hole model is used in combination with an empirical multipole decomposition of the production operator, thus including non-resonant contributions. Our total result in Fig. 19 agrees with the result of these studies with respect to the position of the maximum, but is about 15% higher.

IV. SUMMARY AND CONCLUSIONS

We have presented a relativistic and non-local model for the coherent photoproduction of pions on spin-zero nuclei, which is applicable from threshold up to the Δ-region. Since the calculation for this process is gauge invariant, and since only a minimum amount of theoretical input is needed, this reaction represents an attractive field to test our understandings of hadrons and nuclei.

The production operator was derived from an effective Lagrangian for which the free parameters were fixed by comparison to the data for elementary processes. Applying this production operator to the photoproduction on a nucleus involves an off-shell extrapolation with respect to the nucleon. In our model we used the off-shell behavior following naturally from an effective field theory. The validity of this extrapolation, can only be tested in

comparison to experimental data. Employing a mean field model for the nuclear wave function we neglected higher order effects from many-body correlations.

Our results depend somewhat on the value used for the ωNN coupling constant, which is uncertain by about a factor of two. Employing the same production operator as in vacuum leads to a good reproduction of the shape of the A2 data, but underestimates the absolute value by about a factor of two. Agreement with these data could be achieved by taking into account medium modifications of the production operator via modifications of the nucleon- and Δ-propagators.

We conclude that the relativistic DWIA, employing a realistic production operator is an adequate approach to the coherent photoproduction of pions on nuclei. More experimental data on this process will present a further test of our model and will allow more conclusions about the role of medium effects within our model.

ACKNOWLEDGMENTS

We would like to thank the A2-collaboration at MAMI for providing us with their data prior to publication. We gratefully acknowledge many helpful discussions with R. Shyam in an early stage of this work. We also would like to thank Thomas Feuster for performing the elementary cross section calculations.

REFERENCES

[1] Th. Feuster and U. Mosel, *Nucl. Phys.* **A612**, (1997) 375.

[2] B. Bellinghausen et al., *Z. Phys.* **A309**, (1982) 65, J. Arends et al., *Z. Phys.* **A311**, (1983) 367, G. Tamas et al., *Nucl. Phys.* **A446**, (1985) 327.

[3] R. W. Gothe et al., *Phys. Lett.* **B355**, (1995) 59.

[4] M. Schmitz, Dissertation, Johannes Gutenberg-Universität Mainz, Mainz 1996, to be published.

[5] R.C. Carrasco, J. Nieves and E. Oset, *Nucl. Phys.* **A565**, (1993) 797.

[6] I. Laktineh, W.M. Alberico, J. Delorme and M. Ericson, *Nucl. Phys.* **A555**, (1993) 237.

[7] B. Körfgen, F. Osterfeld and T. Udagawa, *Phys. Rev.* **C50**, (1994) 1637.

[8] E. Oset and W. Weise, *Nucl. Phys.* **A368**, (1981) 375; *Nucl. Phys.* **A402**, (1983) 612.

[9] B. Karaoglu and E.J. Moniz, *Phys. Rev.* **C33**, (1986) 974.

[10] J.H. Koch and E.J. Moniz, *Phys. Rev.* **C27**, (1983) 751.

[11] J.H. Koch and E.J. Moniz, *Phys. Rev.* **C20**, (1979) 235.

[12] A.W. Saharia and R.M. Woloshyn, *Phys. Rev.* **C23**, (1981) 351.

[13] K. Klingenbeck and M.G. Huber, *J. of Phys.* **G6** (1980) 961.

[14] V. Girija, V. Devanathan, A. Nagl and H. Überall, *Phys. Rev.* **C27**, (1983) 1169.

[15] S. Boffi and R. Mirando, *Nucl. Phys.* **A448**, (1986) 637.

[16] S. Boffi L. Bracci and P. Christillin, *Nuovo Cim.* **A104**, (1991) 843.

[17] A.A. Chumbalov, R.A. Eramzhyan and S.S. Kamalov , *Z. Phys.* **A328**, (1987) 195.

[18] A.A. Chumbalov and S.S. Kamalov, *Phys. Lett.* **B196**, (1987) 23, S.S. Kamalov and T.D. Kaipov, *Phys. Lett.* **B162**, (1985) 260.

[19] T. Ericson and W. Weise, *Pions and Nuclei*, Calderon Press, Oxford, 1988

[20] W. Grein and P. Kroll, *Nucl. Phys.* **A338**, (1980) 332.

[21] M. Benmerrouche, N.C. Mukhopadhyay and J.F. Zhang, *Phys. Rev.* **D51**, (1995) 3237.

[22] R.M. Davidson, N.C. Mukhopadhyay and R.S. Wittman, *Phys. Rev.* **D43**, (1991) 71.

[23] O. Dumbrajs et al., *Nucl. Phys.* **B216**, (1993) 277.

[24] H. Garcilazo and E. Moya de Guerra, *Nucl. Phys.* **A562**, (1993) 521.

[25] I. Blomquist and J.M. Laget, *Nucl. Phys.* **A280**, (1977) 405.

[26] D. Menze et al., ZAED Compilation of Pion Photoproduction Data, University of Bonn, 1977.

Landolt-Börnstein *Total Cross Sections for Reactions of High-Energy Particles*, Vol. I/12b, Berlin, 1988.

[27] J. Piekarewicz, A.J. Sarty and M. Benmerrouche, *Phys. Rev.* **C55**, (1997) 2571.

[28] X. Li , L.E. Wright and C. Bennhold, *Phys. Rev.* **C48**, (1993) 816.

[29] L. Tiator and L.E. Wright, *Phys. Rev.* **C30**, (1984) 989.

[30] J.I. Johansson and H.S. Sherif, *Nucl. Phys.* **A575**, (1994) 477.

[31] S. Pollock, H. W. L. Naus and J. H. Koch, *Phys. Rev.* **C53**, (1996) 2304.

[32] A. Gil, J. Nieves and E. Oset , *Nucl. Phys.* **A627**, (1997) 543.

[33] C. J. Joachain, *Quantum collision theory*, 3rd edition, North Holland Physics Publishing, Amsterdam 1983.

[34] G. Audi and A.H. Wapstra, *Nucl. Phys.* **A595**, (1995) 409.

[35] H. de Vries et al., *At. Data Nucl Data Tables* **36** (1987) 495.

[36] C.J. Horowitz and J. Piekarewicz, *Nucl. Phys.* **A511**, (1990) 461.
[37] R.J. Furnstahl and C.E. Price, *Phys. Rev.* **C40**, (1989) 1398.
[38] H. Müther, G. Knehr and A. Polls, *Phys. Rev.* **C52**, (1995) 2995.
[39] H. Lenske and C. Fuchs, *Phys. Lett.* **B345**, (1995) 355; H. Lenske, C. Fuchs and H.H. Wolter, *Phys. Rev.* **C52**, (1995) 3043.
[40] K. Stricker,J.A. Carr and H. McManus, *Phys. Rev.* **C22**, (1980) 2043.
[41] J. A. Carr H. McManus and K. Stricker-Bauer, *Phys. Rev.* **C25**, (1982) 952.
[42] Preedom et al.,*Phys. Rev.* **C23**, (1981) 1134;
Blecher et al., *Phys. Rev.* **C20**, (1979) 1884;
Leitch et al., *Phys. Rev.* **C29**, (1984) 561;
Antonuk et al.,*Nucl. Phys.* **A420**, (1984) 435;
Piffaretti et al., *Phys. Lett.* **B71**, (1977) 324;
Albanese et al., *Nucl. Phys.* **A350**, (1980) 301.
[43] T. Seki and K. Matsutani, *Phys. Rev.* **C27**, (1983) 2799.
[44] C. Garcia-Recio, E. Oset, L.L. Salcedo, D. Strottman and M.J. Lopez, *Nucl. Phys.* **A526**, (1991) 685.
[45] M.B. Johnson and G.R. Satchler, *Ann. of Phys.* **248**, (1996) 134.
[46] E. Oset and L.L. Salcedo, *Nucl. Phys.* **A468**, (1987) 631.
[47] C. Ellegaard et al., *Phys. Rev. Lett.* **59**, (1987) 974.
[48] D. Contardo et al., *Phys. Lett.* **B168**, (1986) 331.
[49] J. Delorme et al., *Phys. Lett.* **B263**, (1991) 157.
[50] T. Udagawa, S.W. Hong and F. Osterfeld, *Phys. Lett.* **B245**, (1990) 1.
[51] N. Bianchi et al., *Phys. Lett.* **B325**, (1994) 333.
[52] M. Effenberger and U. Mosel, *Nucl. Phys.* **A613**, (1997) 353.
[53] B. Krusche, private communication.

TABLES

Nucleus	V_v (MeV)	r_v (fm)	a_v (fm)	V_s (MeV)	r_s (fm)	a_s (fm)
^{12}C	385.7	1.056	0.427	-470.4	1.056	0.447
^{40}Ca	348.1	1.149	0.476	-424.5	1.149	0.506

TABLE I. Strengths, reduced radii and diffusivities for the relativistic scalar and vector mean-field potententials, respectively.

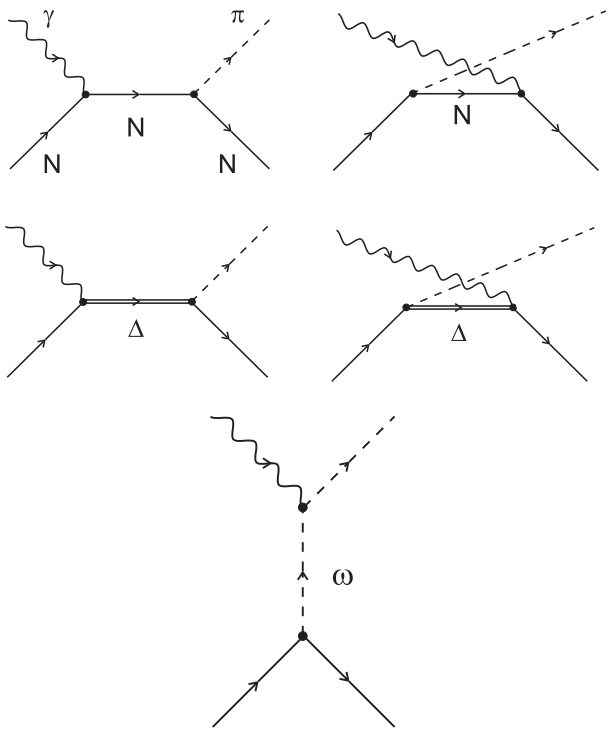

FIG. 1. Feynman diagrams contributing to the photoproduction of neutral pions.

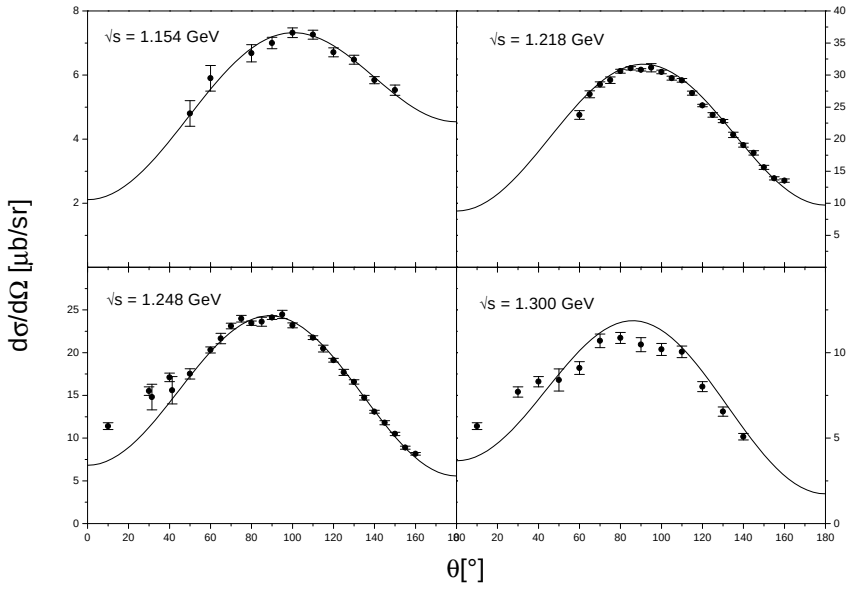

FIG. 2. Differential cross section for $\gamma p \to p\pi^o$ for four different cm-energies $\sqrt{s}$. The data are taken from [26].

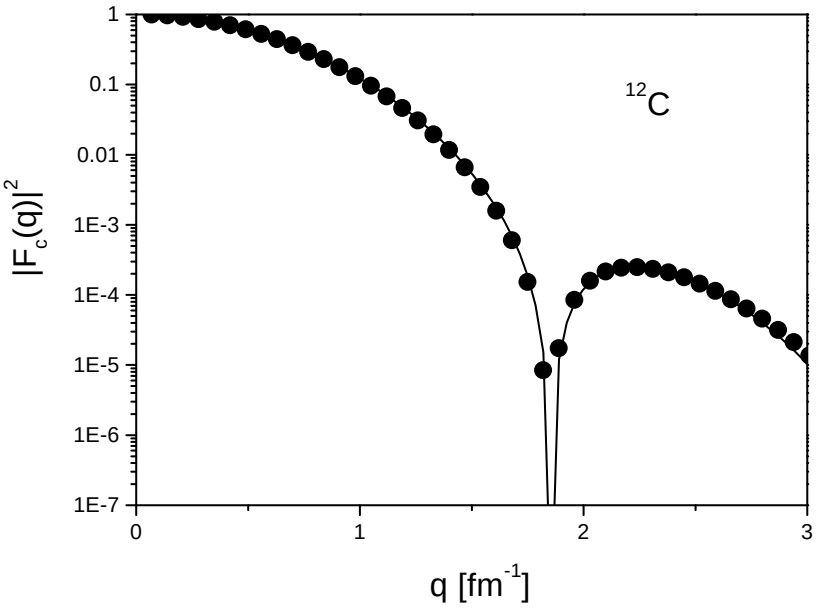

FIG. 3. Charge form factor for ^{12}C resulting from the wave functions used in this work (solid line) in comparison to values extracted from experiment [35] (full circles).

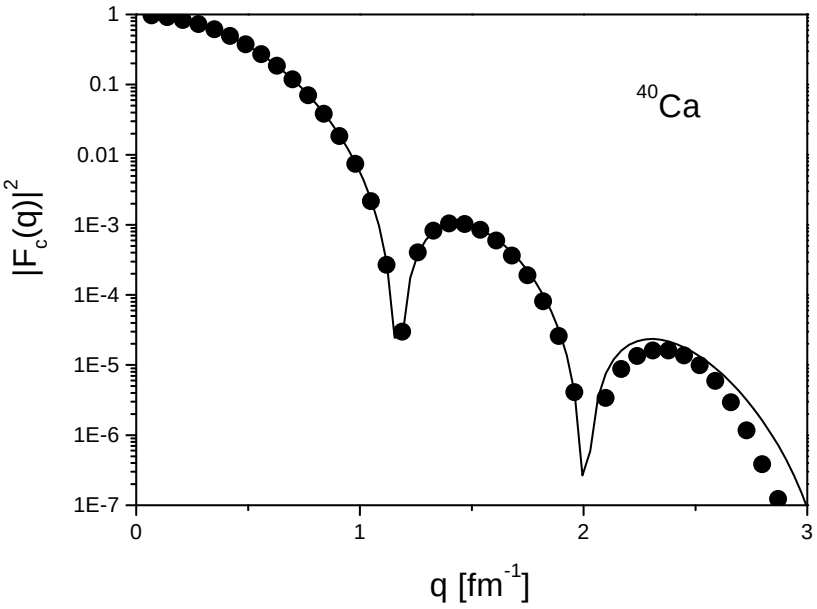

FIG. 4. Same as Fig. 3, but for ^{40}Ca.

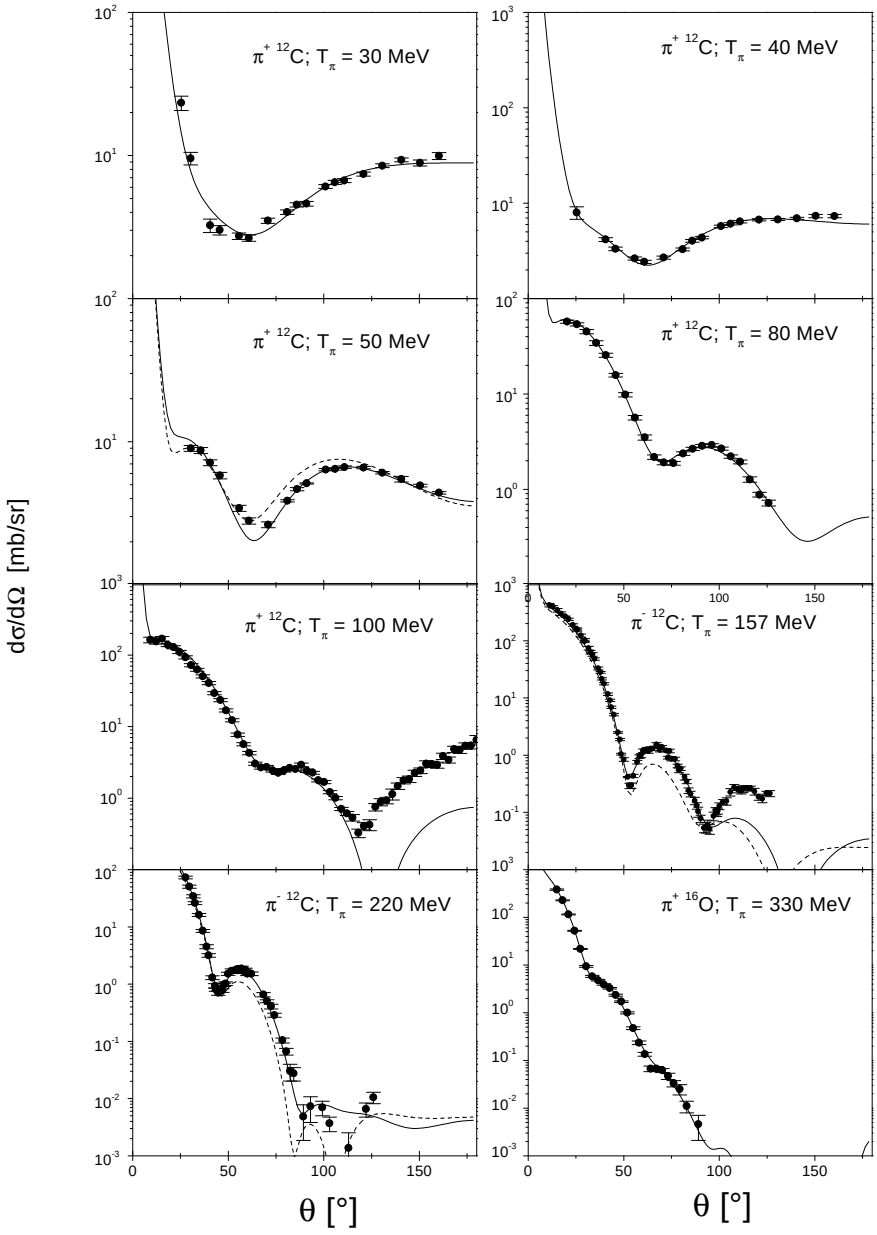

FIG. 5. Fit results for elastic pion scattering as described in the text. The data are taken from Ref. [42]. The dashed lines show results for the parameter set C from [40] at 50 MeV and for the optical potential from [44] at 157 and at 220 MeV.

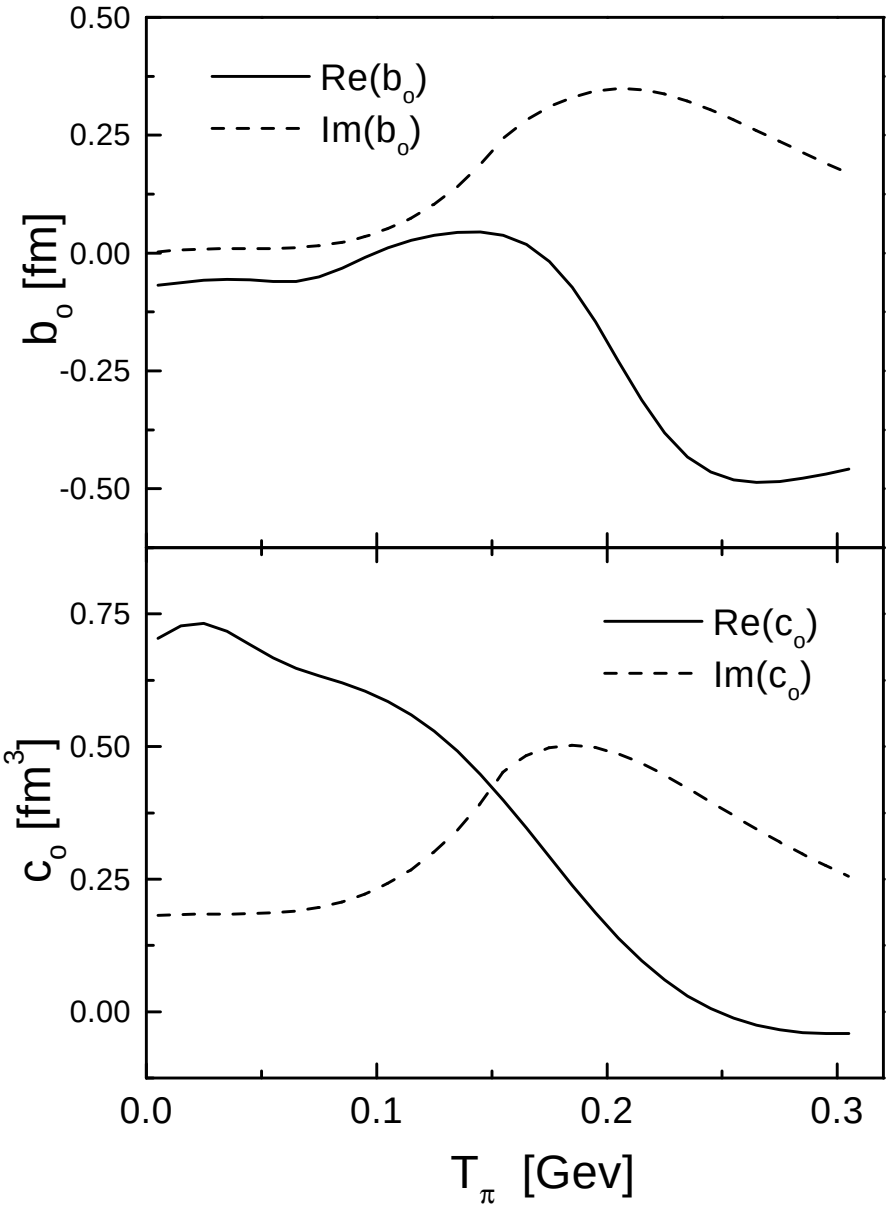

FIG. 6. Energy dependence of the s- and p-wave parameters for the pionic optical potential resulting from our fit as described in the text.

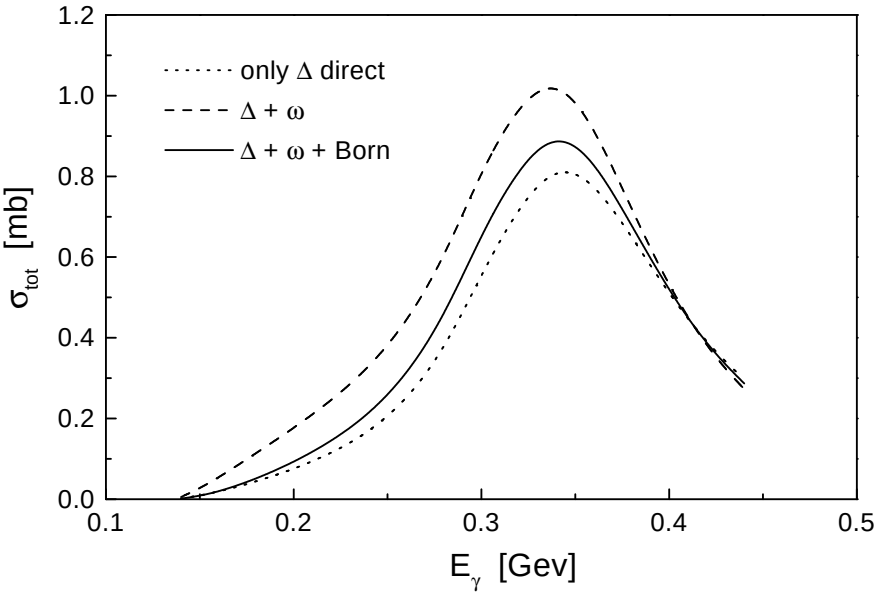

FIG. 7. Contributions of the different fundamental diagrams to the total cross section for $^{12}\mathrm{C}(\gamma,\pi^o)^{12}\mathrm{C}$ in PWIA.

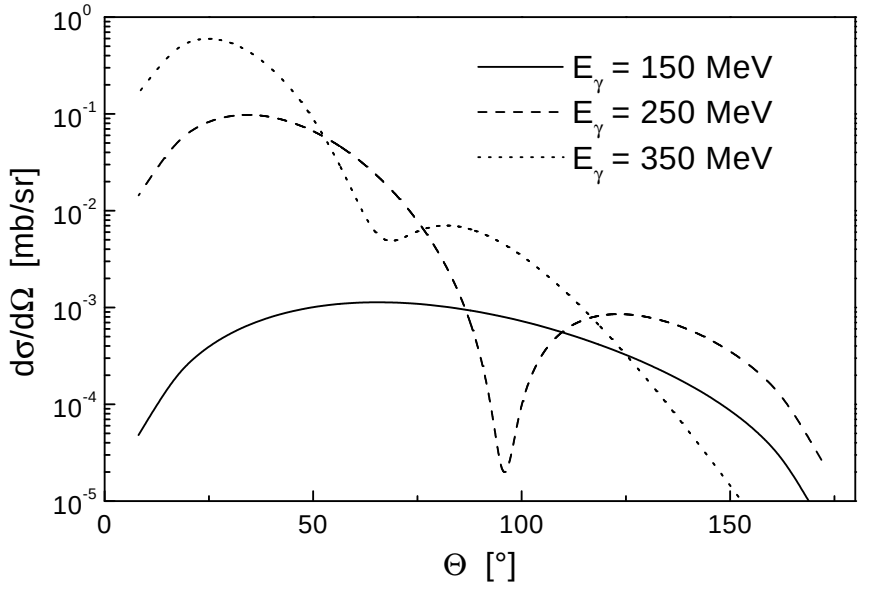

FIG. 8. Differential cross section for $^{12}\mathrm{C}(\gamma,\pi^o)^{12}\mathrm{C}$ in PWIA for three different energies.

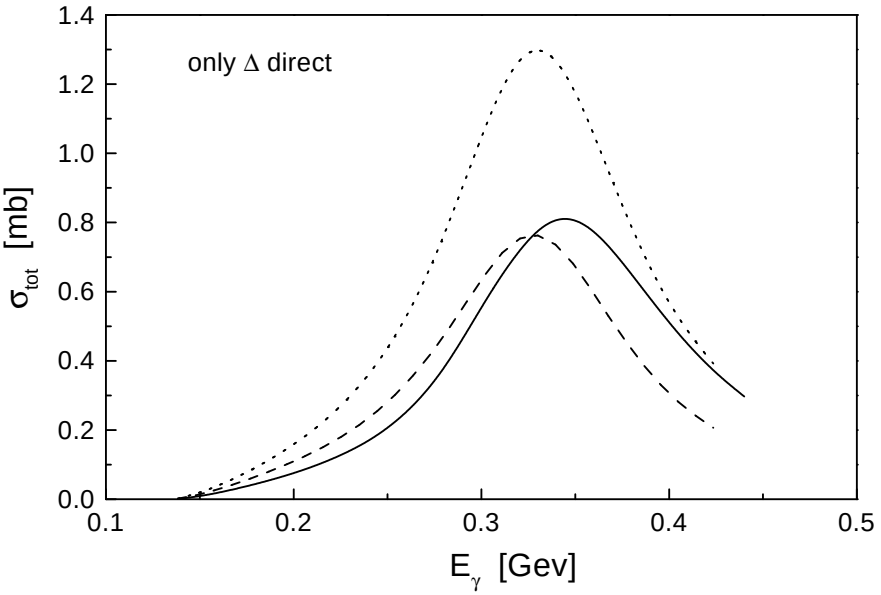

FIG. 9. Total cross section for ^{12}C$(\gamma,\pi^o)^{12}$C in PWIA resulting from the direct Δ-graph (solid line) in comparison to non-relativistic, local calculations as in [15,17] (dotted line) and including the kinematical correction from [5] (dashed line) as described in the text.

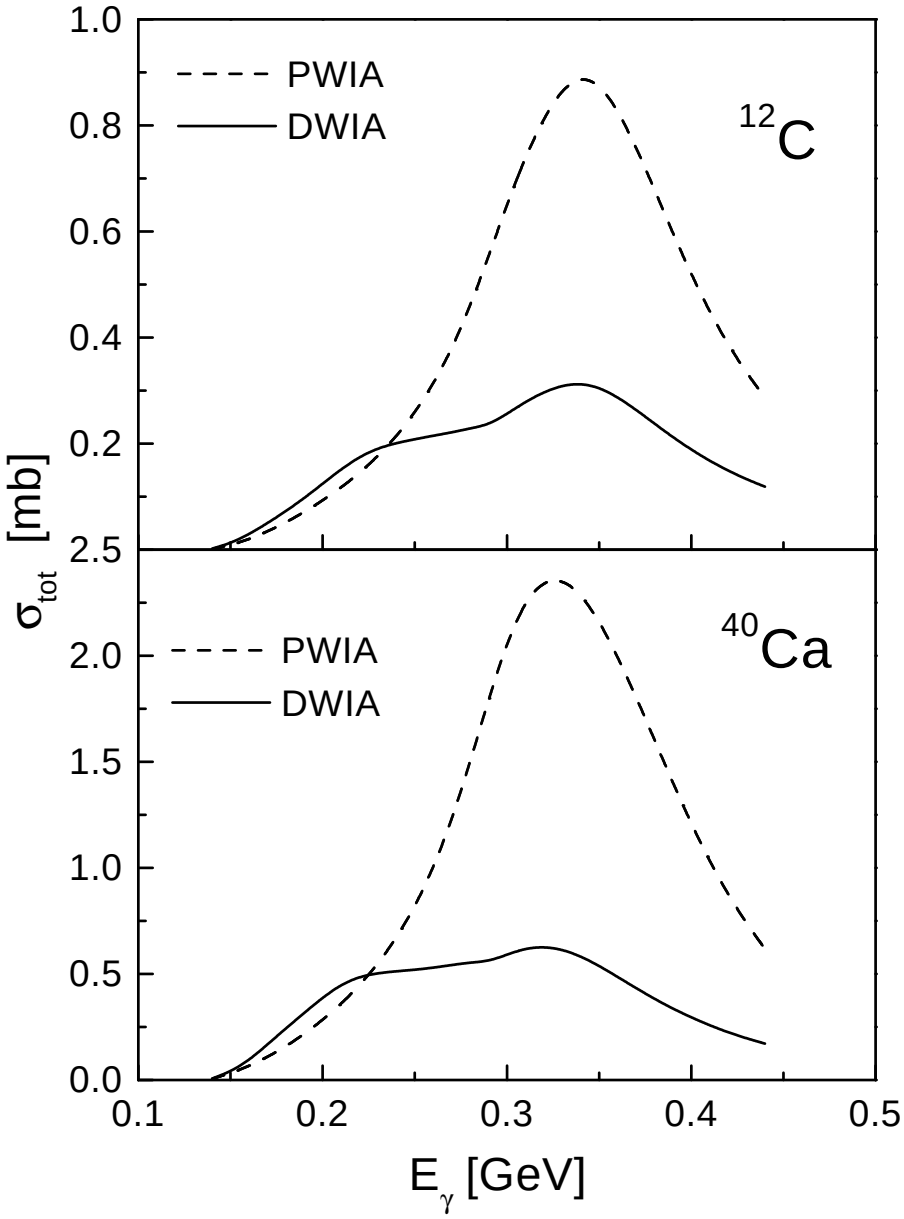

FIG. 10. Total cross section in DWIA and PWIA for $^{12}\mathrm{C}(\gamma,\pi^o)^{12}\mathrm{C}$ and $^{40}\mathrm{Ca}(\gamma,\pi^o)^{40}\mathrm{Ca}$.

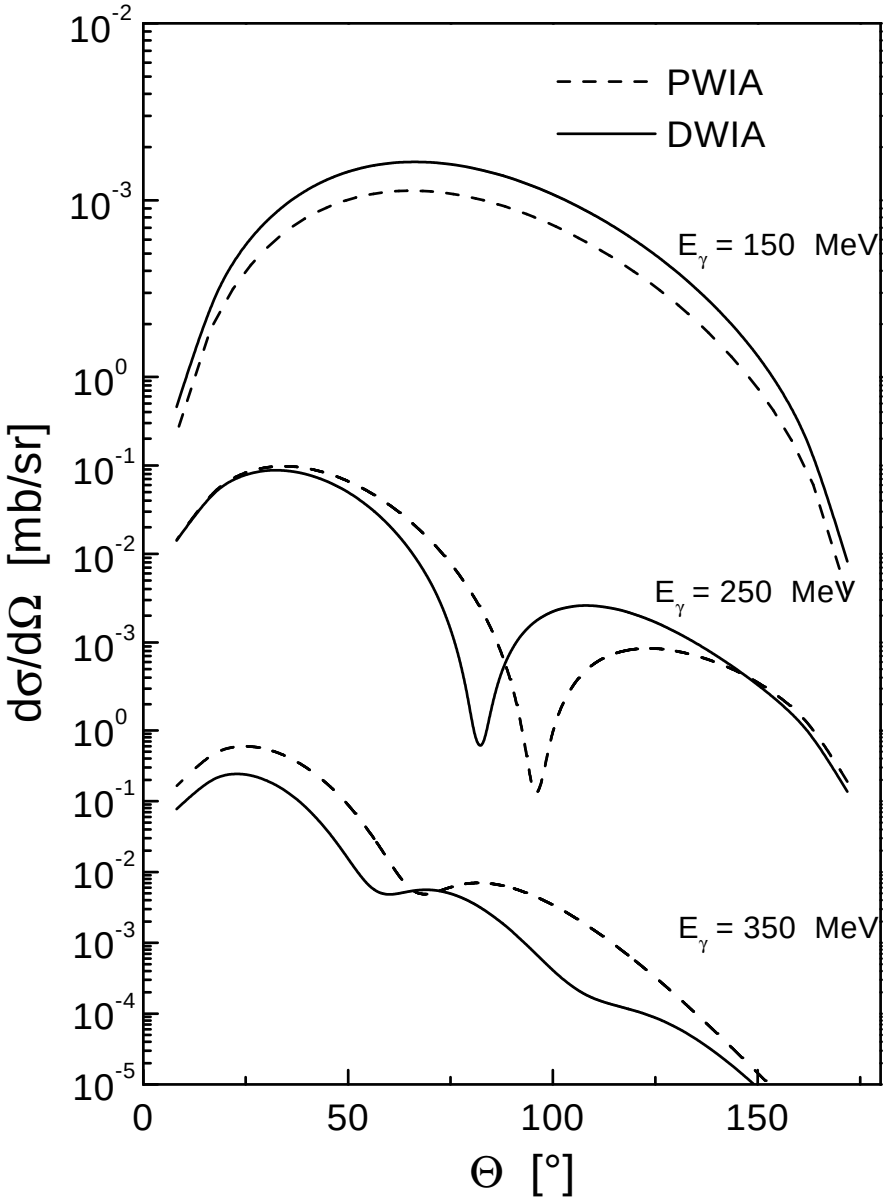

FIG. 11. Differential cross section in DWIA and PWIA for ^{12}C$(\gamma, \pi^o)^{12}$C.

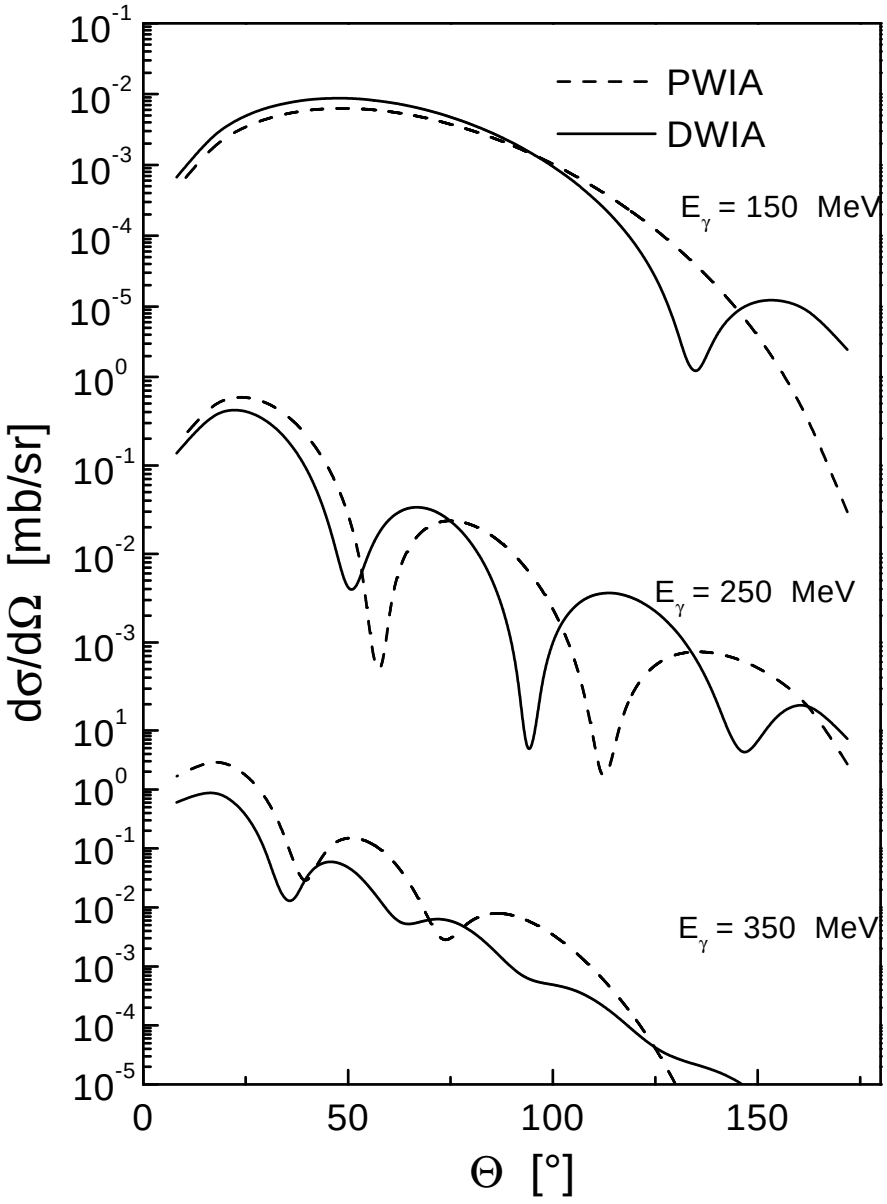

FIG. 12. Differential cross section in DWIA and PWIA for ^{40}Ca$(\gamma, \pi^o)^{40}$Ca.

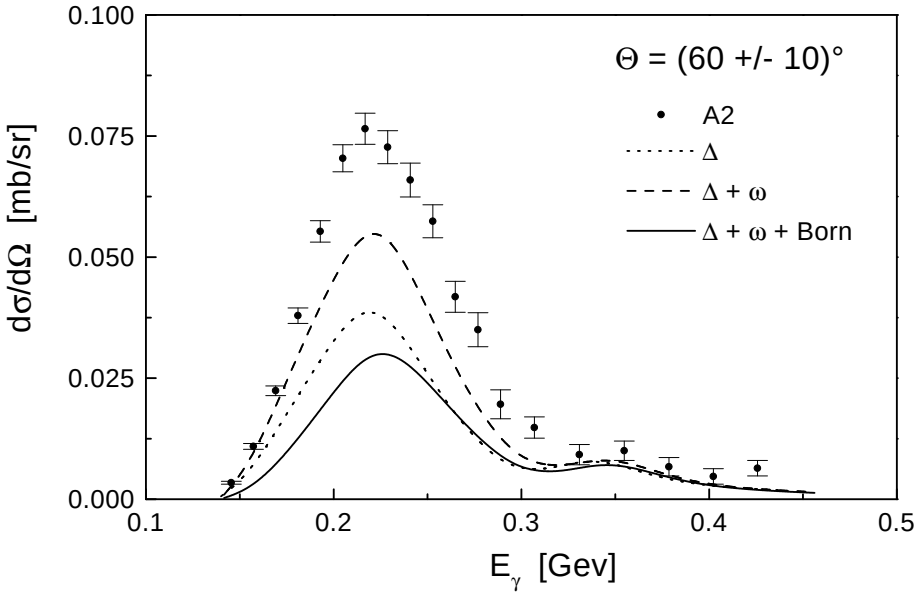

FIG. 13. Comparison of the A2-data for ^{12}C to a DWIA calculation.

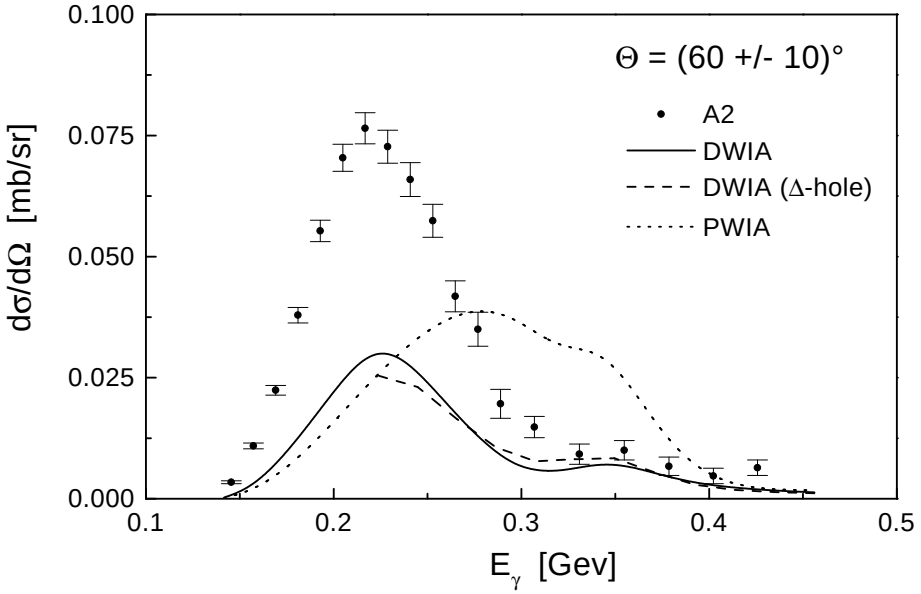

FIG. 14. Comparison of the A2-data for ^{12}C to DWIA calculations employing two different optical potentials and a PWIA calculation.

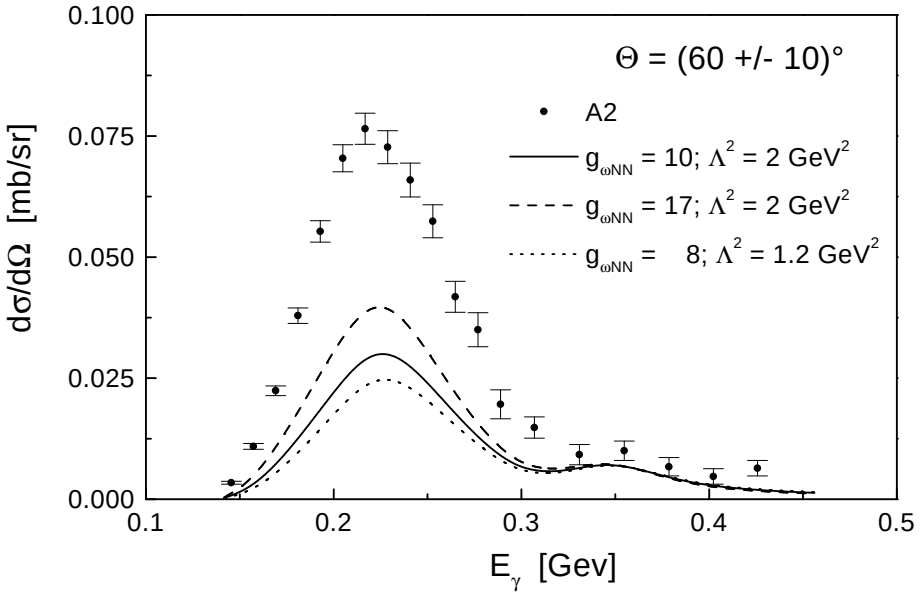

FIG. 15. Comparison of the A2-data for ^{12}C to DWIA calculations employing different ωNN couplings and cutoffs. The solid curve was obtained with the values used throughout this work.

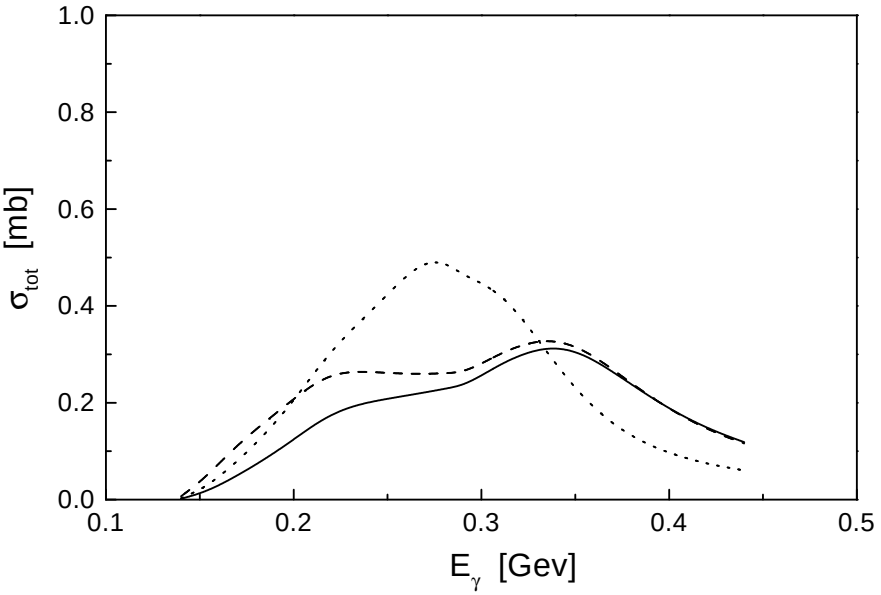

FIG. 16. Total DWIA cross section for $^{12}\mathrm{C}(\gamma,\pi^o)^{12}\mathrm{C}$ using the free production operator (full line), using the dressed nucleon propagator (dashed line) as described in the text, and with a mass shift of the Δ δm_Δ = -30 MeV (dotted line).

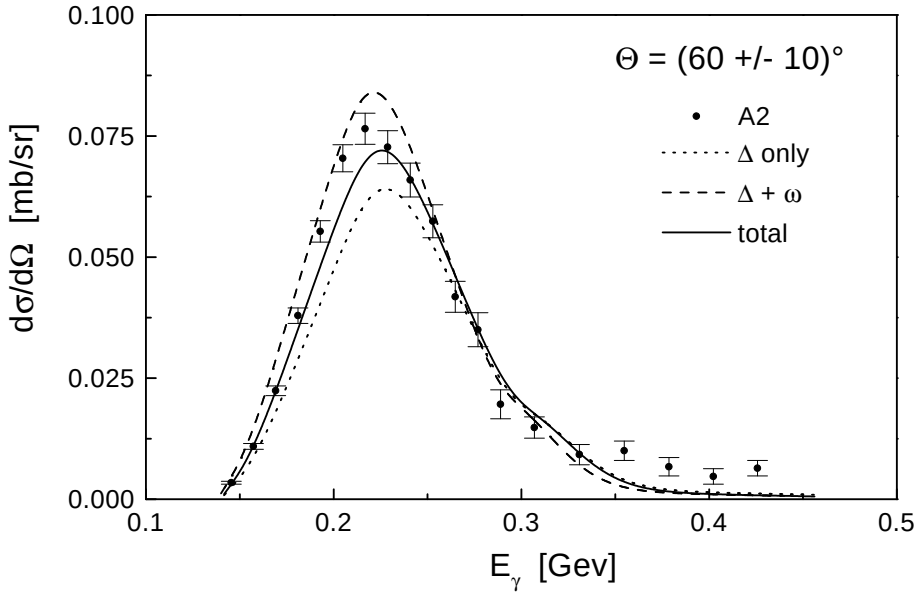

FIG. 17. Comparison of the A2-data for ^{12}C to a DWIA calculation employing a medium-modified production operator with a dressed nucleon propagator and a shifted Δ-mass (δm_Δ=-30 MeV).

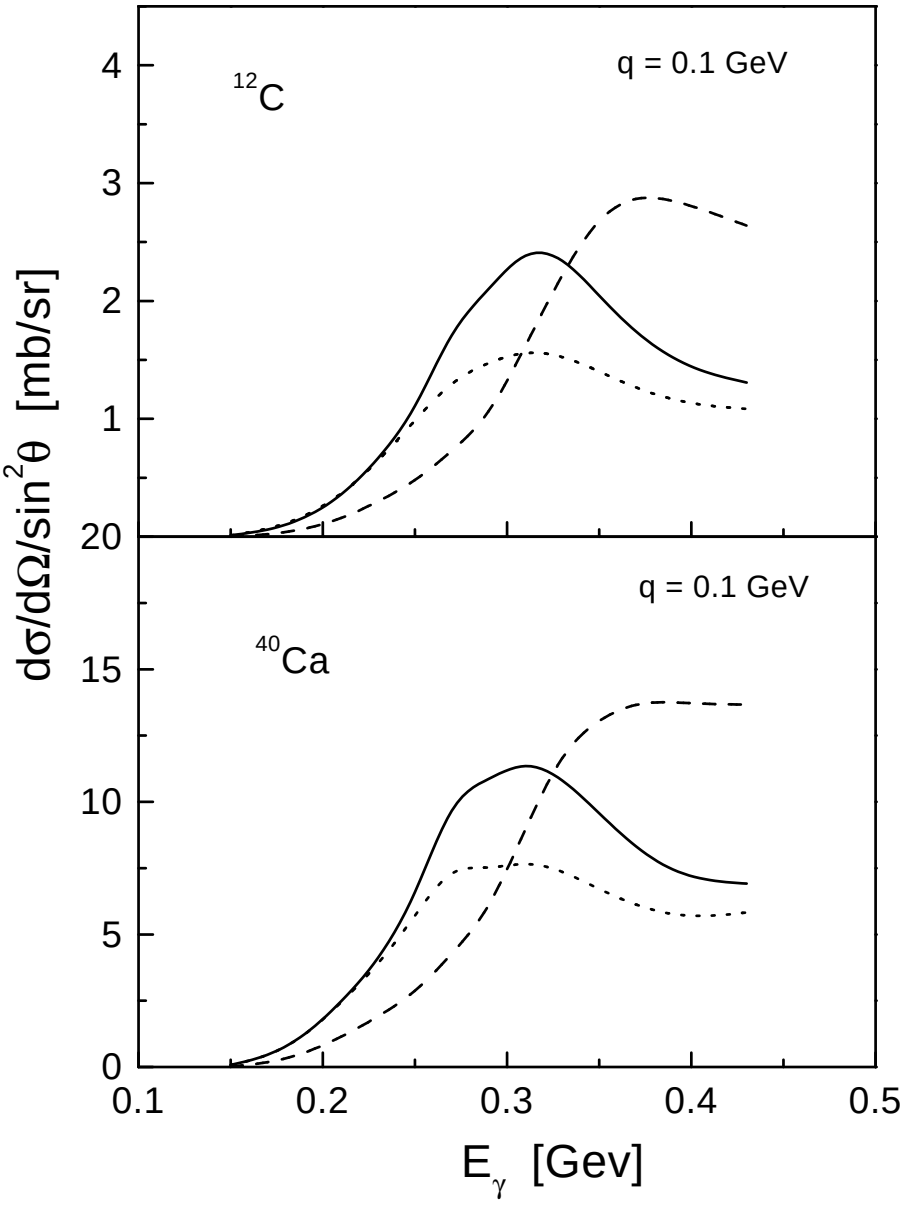

FIG. 18. Differential cross section divided by $\sin^2\theta$ for $^{12}\mathrm{C}(\gamma,\pi^o)^{12}\mathrm{C}$ and $^{40}\mathrm{Ca}(\gamma,\pi^o)^{40}\mathrm{Ca}$ for a fixed momentum transfer of 0.1 GeV: free production operator (dashed line), in-medium production operator with a dressed nucleon propagator and a Δ-mass shift δm_Δ=-30 MeV (full line), and with an in-medium production operator including additionally an increased Δ-width $\delta\Gamma_\Delta$ = 30 MeV (dotted line).

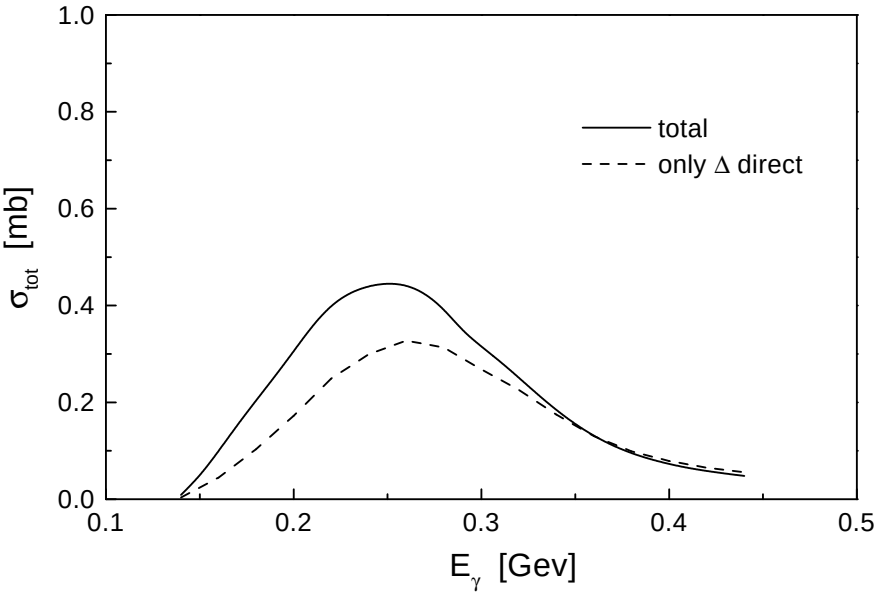

FIG. 19. Total cross section for $^{12}\mathrm{C}(\gamma,\pi^o)^{12}\mathrm{C}$ using an in-medium production operator (δm_Δ=-30 MeV, $\delta\Gamma_\Delta$ = 30 MeV), for a complete calculation, as well as for a calculation where only the direct Δ-graph is included.